Nationaal Lucht- en Ruimtevaartlaboratorium
National Aerospace Laboratory NLR

NLR TP 96288

Adaptive 3D Single-Block Grids for the Computation of Viscous Flows around Wings

R. Hagmeijer and J.C. Kok

DOCUMENT CONTROL SHEET

	ORIGINATOR'S REF.		SECURITY CLASS.
	NLR TP 96288 U		**Unclassified**

ORIGINATOR
National Aerospace Laboratory NLR, Amsterdam, The Netherlands

TITLE
Adaptive 3D single-block grids for the computation of viscous flows around wings

PRESENTED AT
The 5th International Conference on Numerical Grid Generation in Computational Fluid Dynamics and Related Fiels, April 1-5, 1996, Starkville, Mississippi.

AUTHORS	DATE	pp	ref
R. Hagmeijer, J.C. Kok	**960424**	**14**	**12**

DESCRIPTORS

Adaption
Aerodynamic coefficients
Algorithms
Boundary conditions
Grid generation (mathematics)
Navier-Stokes equation
Reynolds number
Structured grids (mathematics)
Three dimensional flow
Transonic flow
Wings

ABSTRACT
A robust algorithm for the adaptation of a 3D single-block structured grid suitable for the computation of viscous flows around a wing is presented and demonstrated by application to the ONERA M6 wing. The effects of grid adaptation on the flow solution and acuracy improvements are analyzed. Reynolds number variations are studied.

Adaptive 3D Single-Block Grids for the Computation of Viscous Flows around Wings

R. Hagmeijer
J.C. Kok

National Aerospace Laboratory NLR
P.O. Box 90502, 1006 BM Amsterdam, The Netherlands
phone 31-20-5113459, fax 31-20-5113210, email: hagm@nlr.nl, jkok@nlr.nl

Abstract

A robust algorithm for the adaption of a 3D single-block structured grid suitable for the computation of viscous flows around a wing is presented and demonstrated by application to the ONERA M6 wing. The effects of grid adaption on the flow solution and acuracy improvements are analyzed. Reynolds number variations are studied.

Introduction and objectives

The motivation for the development of automatically adapted grids within the field of computational fluid dynamics (CFD) consists of two parts [1]:

1. The numerical solution to a specific problem should be achieved with the lowest possible number of degrees of freedom, given the accuracy of the flow solver and the desired or required accuracy of the flow solution.

2. The construction of a suitable grid for the problem at hand should not be done by hand but by means of an algorithm.

Part 1 of this motivation addresses the computing time that are associated with large scale computations. Flow calculations based on solution of the Navier-Stokes equations require several millions of degrees of freedom and are constrained by the memory limits of today's supercomputers. Part 2 of this motivation addresses the turnaround time needed for the solution of real-life realistic aerodynamic problems concerning the design of aircraft configurations. Presently the turnaround time for such problems typically is in the order of several months, primarily needed for the generation of a high-quality structured grid, depending on the complexity of the problem at hand. In order to efficiently contribute to aircraft design the problem-turnaround time must be reduced to the order of a day or a week [2].

The first objective of the present paper is to present the development of a robust algorithm for the adaption of a 3D single-block structured grid suitable for the com-

putation of viscous flows around a wing. The algorithm is robust in the sense that it can be applied automatically without user interaction. Since the number of nodes is fixed during adaption, the goal of the algorithm is to distribute the available nodes over the computational domain in some optimal sense. The second objective is to demonstrate application to a 3D test case consisting of calculation of the viscous flow around a transonic wing-alone configuration. The third objective is to analyse the effects of grid adaption on the flow solution and to assess the acuracy improvements.

Mathematical model used for grid adaption

Let $\mathbf{x}(\mathbf{p}) : \ \Omega_p = [0,1]^3 \mapsto \Omega \subset \mathbf{R}^3$ be the map that defines the initial grid in physical space as the image of a uniform grid in the unit cube Ω_p, called the parametric domain. In the same way let $\mathbf{x}_a(\xi) : \ \Omega_c = [0,1]^3 \mapsto \Omega \subset \mathbf{R}^3$ be the map that defines the adapted grid in physical space as the image of a uniform grid in the unit cube Ω_c, called the computational domain. As a direct extension of the 2D developments in [3] the adaptive map $\mathbf{x}_a(\xi)$ is defined in terms of the initial map: $\mathbf{x}_a(\xi) = \mathbf{x}(\mathbf{p}(\xi))$. Hence the goal is to define an adaptive map $\mathbf{p}(\xi)$ between the parametric domain Ω_p and the computational domain Ω_c. In [3] the partial differential equations that are used to define the adaptive map $\mathbf{p}(\xi)$ are basically derived from a variational problem formulation.

The complete boundary value problem formulation for adaptive grid generation is conveniently formulated in the parametric domain Ω_p, based on minimization of a weighted least squares (WLS) functional:

$$K[\xi,\eta,\zeta] = \frac{1}{2}\int_{\Omega_p}\left\{\frac{\|\xi_p\|^2}{w_1} + \frac{\|\xi_q\|^2}{w_2} + \frac{\|\xi_r\|^2}{w_3}\right\} d\Omega_p, \quad \xi = (\xi,\eta,\zeta)^T, \tag{1}$$

where ξ_p indicates differentiation of the vector $\xi = (\xi,\eta,\zeta)^T$ to p etc., $\|.\|$ denotes the Eucledian norm and $w_i,\ i = 1,2,3$, are weight functions that measure the flow solution gradients. For background information with respect to the formulation of the functional K the reader is refered to [3]. To ensure that the adapted grid in the physical domain be boundary conforming a set of essential boundary conditions is imposed:

$$\begin{array}{l} \xi(0,q,r) = 0,\ \xi(1,q,r) = 1, \\ \eta(p,0,r) = 0,\ \eta(p,1,r) = 1, \\ \zeta(p,q,0) = 0,\ \zeta(p,q,1) = 1. \end{array} \tag{2}$$

To solve the variational problem (1) and (2), the associated EL equations

$$L[\xi^{(k)}] \equiv \frac{\partial}{\partial p}(\frac{\xi_p^{(k)}}{w_1}) + \frac{\partial}{\partial q}(\frac{\xi_q^{(k)}}{w_2}) + \frac{\partial}{\partial r}(\frac{\xi_r^{(k)}}{w_3}) = 0,\ k = 1,2,3, \tag{3}$$

must be solved and a set of additional natural boundary conditions must be satisfied:

$$\begin{array}{l} \xi_q(p,0,r) = 0,\ \xi_q(p,1,r) = 0,\ \xi_r(p,q,0) = 0,\ \xi_r(p,q,1) = 0, \\ \eta_p(0,q,r) = 0,\ \eta_p(1,q,r) = 0,\ \eta_r(p,q,0) = 0,\ \eta_r(p,q,1) = 0, \\ \zeta_p(0,q,r) = 0,\ \zeta_p(1,q,r) = 0,\ \zeta_q(p,0,r) = 0,\ \zeta_q(p,1,r) = 0. \end{array} \tag{4}$$

The weight functions w_i are defined as functions of a monitor function $\mathbf{Q}(\mathbf{p})$:

$$w_i(\mathbf{p}) = \|\frac{\partial \mathbf{Q}}{\partial p_i}\|,\ \mathbf{Q} \in \mathbf{R}^N,\ N \geq 1. \tag{5}$$

In [3] $\mathbf{Q}(\mathbf{p})$ was defined for 2D problems as $\mathbf{Q}(\mathbf{p}) = (p, q, Q^{(1)}, ..., Q^{(n)})^T$ where $Q^{(k)},\ k = 1, ..., n$ represent components of the flow solution. The presence of p and q, which are the parametric coordinates for 2D problems, provides that the initial grid is preserved when the conservative variables are bi-linear functions of p and q. For 3D problems the monitor function can be chosen as:

$$\mathbf{Q}(\mathbf{p}) = (p, q, r, \rho, \rho u, \rho v, \rho w, \bar{p})^T, \tag{6}$$

where the last five components represent mass per unit volume, momentum in x,y,z directions and static pressure respectively. Taking a relatively large set of monitor function components in stead of only two (e.g. the Mach number and the pressure coefficient) has the advantage that gradients in the flow solution have a much larger chance to be represented by the weight functions.

In [3] a 2D analysis shows that skewness of the adapted grid in the parametric domain is amplified upon mapping to the physical domain if the initial grid in the physical domain possesses cells with large aspect ratios. A modification of the EL equations was proposed resulting in the so-called modified anisotropic diffusion (MAD) equations. Again a direct extension for the 3D development can be obtained:

$$\tilde{L}[\xi^{(k)}] = \lambda_1 \frac{\partial}{\partial p}(\frac{\xi_p^{(k)}}{w_1}) + \lambda_2 \frac{\partial}{\partial q}(\frac{\xi_q^{(k)}}{w_2}) + \lambda_3 \frac{\partial}{\partial r}(\frac{\xi_r^{(k)}}{w_3}) = 0,\ k = 1, 2, 3, \tag{7}$$

where the modification functions $\lambda_i,\ i = 1, 2, 3$ are defined as:

$$\lambda_i(\mathbf{p}) = w_i^2 \|\mathbf{x}_{p^j}\|^2 \|\mathbf{x}_{p^k}\|^2, \quad i, j, k \ \ cyclic. \tag{8}$$

A critical issue of grid generation and grid adaption is that the underlying map be invertible. In view of this it is important to note that if the above defined boundary value problem reduces to a 2D problem (e.g. if the derivatives of w_i and λ_i with respect to r are zero) then the recently formulated theorem in [6] assures that the map $\mathbf{p}(\xi)$ is regular in the sense that it is C^2 and one-to-one and the Jacobian is positive everywhere. Unfortunately until date such theorem has not been developed yet for the 3D problem.

In Fig. 1 the CO-topology of a single block around a wing is depicted as a map from the unit cube. The central part of the lower face of the cube is mapped to the wing surface while the remaining parts of the lower face are mapped to the upper and lower side of the wake cut respectively. The back face of the cube is mapped to the upper and lower side of the horizontal plane outside the wing. Hence two face-to-face connections are present: the off-centre parts of the downward face and the two halfs of the back face.

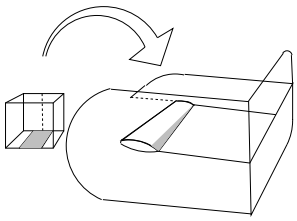

Figure 1: Single block CO-topology

The adaption of this single block topology is performed in steps [3]. First the basic adaption map is applied by solving the MAD equations. The MAD equations are discretised by means of central differences and the resulting large linear system is solved by means of GMRES relaxation [7]. The specific GMRES algorithm has been taken from the netlib.linalg library (ftp address: netlib2.cs.utk.edu) provided by the University of Tennessee and Oak Ridge National Laboratory. A correction storage multi-grid technique [8] with fixed V-cycles is used to increase the rate of convergence. Subsequently the lower and back faces are corrected to satisfy the face-to-face connection requirements. Then both corrected faces are matched on the common edge. Finally the block interior is matched to the corrected faces. The result is the inverse adaption map $\xi(\mathbf{p})$. To re-invert this map to the adaption map $\mathbf{p}(\xi)$ each of the rectangular cells in the uniform 3D grid in the parametric domain Ω_p is subdivided into six tetrahedra. Then in a loop over these tetrahedra the values of ξ, η and ζ are examined at the vertices resulting in a number of candidate new grid points that may be present in the specific tetrahedron. The final presence check only involves some basic linear algebra if all functions on the tetrahedron are linearly approximated.

Results for ONERA M6 wing

To illustrate the grid adaption algorithm we present calculations for the ONERA M6 wing under transonic flow conditions [9]. We have performed calculations on both non-adapted and adapted grids, medium and fine grids, and for three different Reynolds numbers, see table 1. For all calculations we have used the NLR flow simulation system ENFLOW, [10],[11],[12], to solve the Thin-layer approximation of the Reynolds-averaged Navier-Stokes equations including the Baldwin-Lomax turbulence model, or to generate grids. Fig. 2 shows the medium grid (Fig. 2a)

Table 1: Calculated cases for ONERA M6 wing (n=non-adapted, a=adapted), $M_\infty = 0.84$,$\alpha = 3.06^\circ$.

	dimensions	$Re_\infty = 3 \cdot 10^6$	$Re_\infty = 11.7 \cdot 10^6$	$Re_\infty = 48 \cdot 10^6$
medium	128x24x32	n+a	n+a	n+a
fine	256x48x64	n	n	n

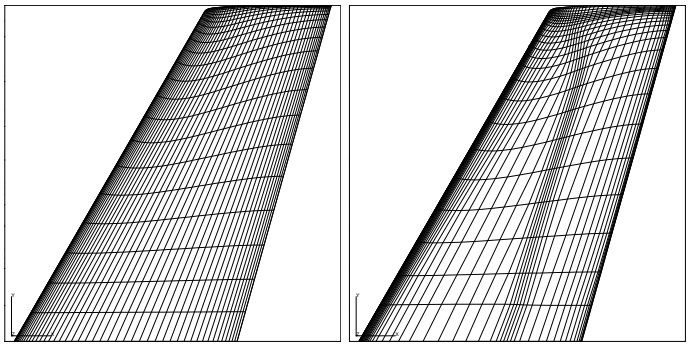

a) non-adapted grid b) adapted grid

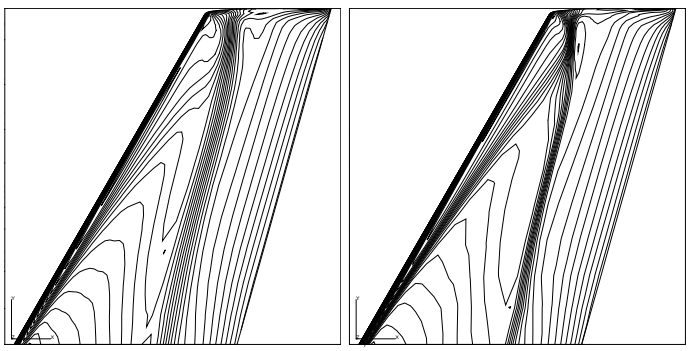

c) C_p on non-adapted grid d) C_p on adapted grid

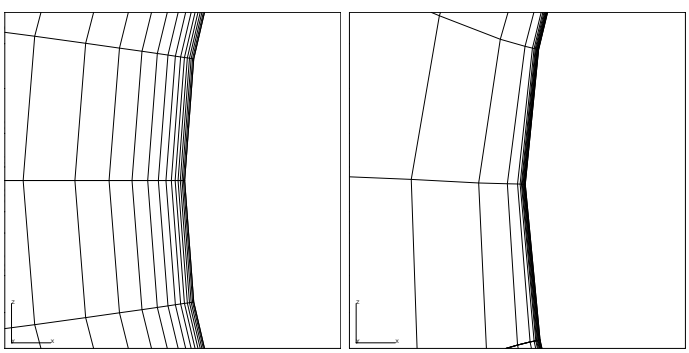

e) non-adapted grid, nose f) adapted grid, nose

Figure 2: Non-adapted and adapted medium grid (a),(b), and C_p-distributions (c) and (d) on wing upper surface, and close-ups of non-adapted and adapted grid near the leading edge in the root plane, $Re_\infty = 11.7 \cdot 10^6$.

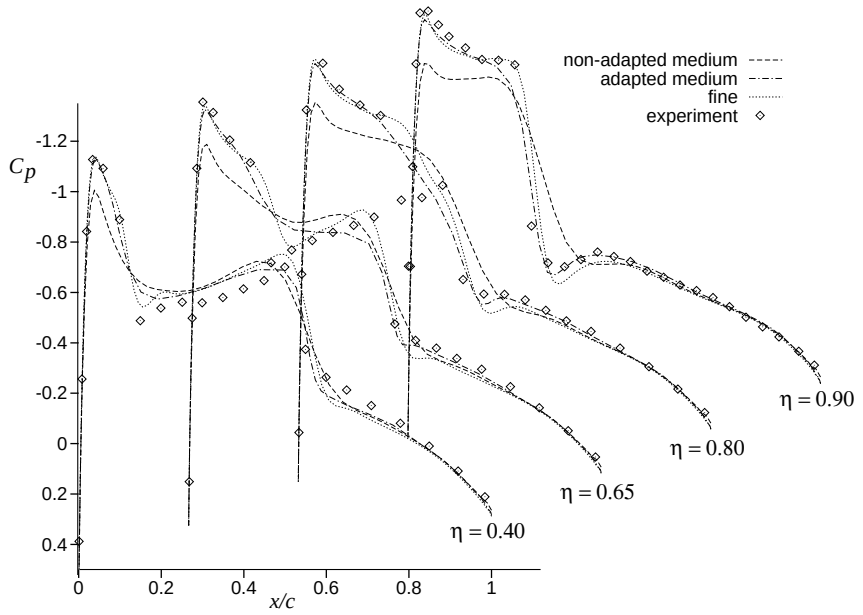

Figure 3: Pressure distributions (C_p) on non-adapted and adapted grids compared to fine grid result and experimental data, $Re_\infty = 11.7 \cdot 10^6$.

and the adapted medium grid (Fig. 2b) and the calculated pressure coefficient (C_p) distributions (Fig. 2c and 2d). Adaption at the leading edge, trailing edge, shock position and tip are visible resulting in a more pronounced shock. Details of the adaption near the nose at the symmetry plane (Fig. 2e and 2f) show concentration at the boundary layer with a non-smooth transition to the outer flow. The C_p distributions at the upper side of various cross sections of the wing are depicted in more detail in Fig. 3 and compared to the fine grid result and experimental data. The suction peak at the leading edge and the down stream expansion zone from the fine grid result and the experimental data is completely recovered by the adapted medium grid result, while the non-adapted medium grid result fails in this respect. The lower side distributions (not shown) show the same features. The skin-friction (C_f) distributions at the upper side of various cross sections of the wing are depicted in Fig. 4 for the $Re_\infty = 48 \cdot 10^6$ calculation. Along the complete upper side adaption results in significant improvements. Also it is visible how the laminar-turbulent transition line has shifted upstream upon adaption due to the fact that the flow solver uses grid line indices for transition indication. Less pronounced effects are encountered for the lower two Reynolds numbers (not shown). The influence of grid adaption on the boundary layer resolution is explicitly demonstrated in Fig. 5 showing the 'Law-of-the-wall' coordinate Y^+ of the first grid point above the wing surface at the 65% span cross section. For the $Re_\infty = 11.7 \cdot 10^6$ case the Y^+ distribution over the grid is significantly improved upon adaption compared to the

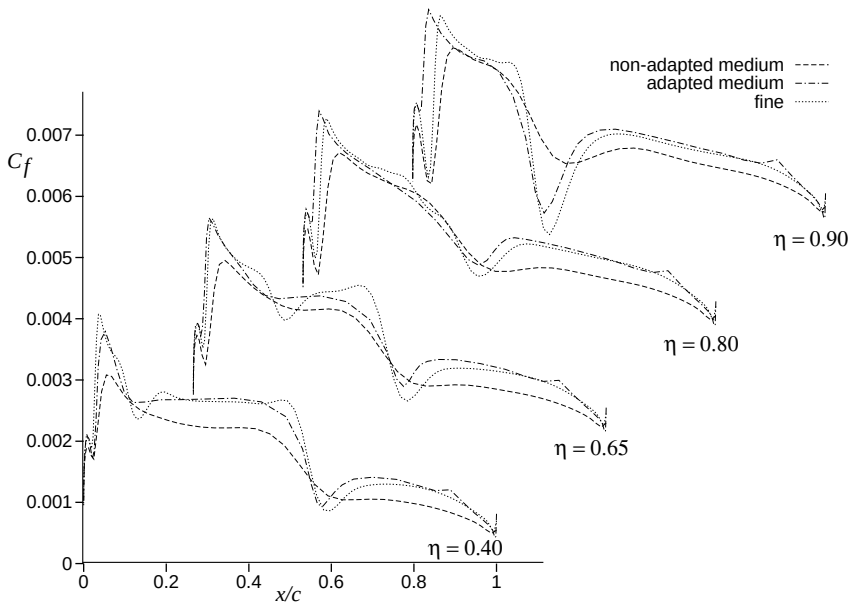

Figure 4: Skin-friction distribution on non-adapted and adapted grids compared to fine grid result, $Re_\infty = 48 \cdot 10^6$

fine grid result. For the $Re_\infty = 48 \cdot 10^6$ case the improvement is even stronger: the adapted medium grid resolves the boundary layer better than the fine grid and the Y^+ values are roughly reduced by 30%. The stronger effect for the high Reynolds number case is not unexpected since the initial grids have been generated for the $Re_\infty = 11.7 \cdot 10^6$ case by CFD experts with a state-of-the-art elliptic grid generator. From Fig. 5a we learn that even such a special purpose grid can be automatically modified to improve the Y^+ resolution by roughly 50%. The influence of grid adaption on the aerodynamic coefficients is shown in Fig. 6 which shows the lift (C_L), drag (C_D), friction drag (C_{D_f}), and pitching moment (C_{M_p}) coefficients respectively as calculated on the non-adapted and adapted medium grids, and on the fine grid, for three different Reynolds numbers. Globally grid adaption results in improvement of the coefficient predictions if compared to the fine grid results. More specifically the drag coefficient, see Fig. 6b, is strongly improved: the gap of 25 counts between the medium and fine grid results is reduced to 6 counts upon grid adaption. This is still too large for practical problems but it should be reminded that the medium grid only consists of about 100,000 points. For $Re_\infty = 48 \cdot 10^6$ the friction drag is strongly improved upon grid adaption, see Fig. 6c. Besides the absolute values of the predictions it is remarkable that the adapted medium grid results and the fine grid results have almost the same dependency on the Reynolds number and only differ by a constant for all four coefficients. This is not true for the non-adapted medium grid result.

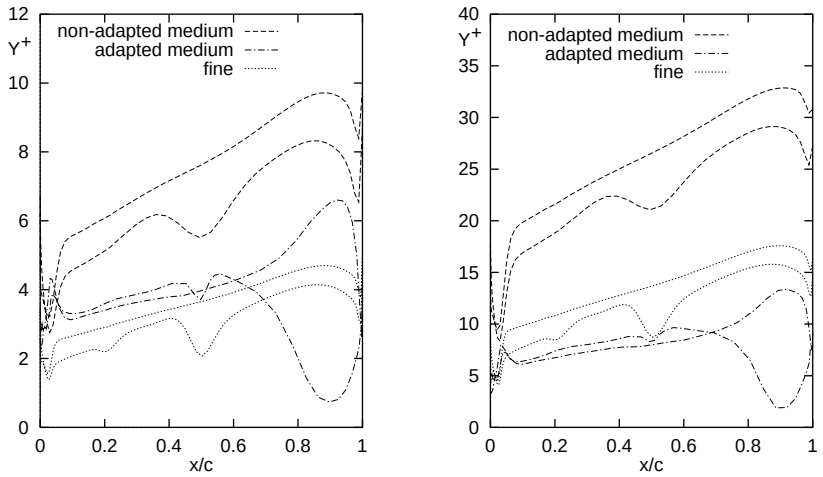

a) $Re = 11.7 \cdot 10^6$ b) $Re = 48 \cdot 10^6$

Figure 5: Law-of-the-wall coordinate of first grid point above the surface at 65% span cross section on various grids.

Conclusions

The presented adaption algorithm for structured 3D single-block grids appears to be robust in the sense that it fully automatically generates heavily adapted grids which are regular and non-overlapping. Adaption of single-block structured grids of approximately 100,000 points around the ONERA M6 wing shows significant improvement of the flow solution: both the pressure and skin-friction distributions improve if compared to a fine grid result. Specifically the suction peak at the wing leading edge calculated on the fine grid is completely recovered by the adapted medium grid result, and the skin friction distributions approximate the fine grid result closely. Three main nconclusions can be drawn:

1. The grid adaption algorithm enables flow calculations with improved accuracy,
2. The grid adaption algorithm enables automatic construction of a suitable grid for a wide range of Reynolds numbers,
3. The grid adaption algorithm enables an improved estimate of the influence of Reynolds number variations on the aerodynamic coefficients.

The second conclusion is based on the fact that the non-adapted grid has been generated for the $Re_\infty = 11.7 \cdot 10^6$ case but upon adaption can easily be used for Reynolds numbers that differ by a factor of four. The third conclusion is based on the fact that the adapted medium grid results and the fine grid results show identical variations of the aerodynamic coefficients as a function of the Reynolds number and only differ by a constant.

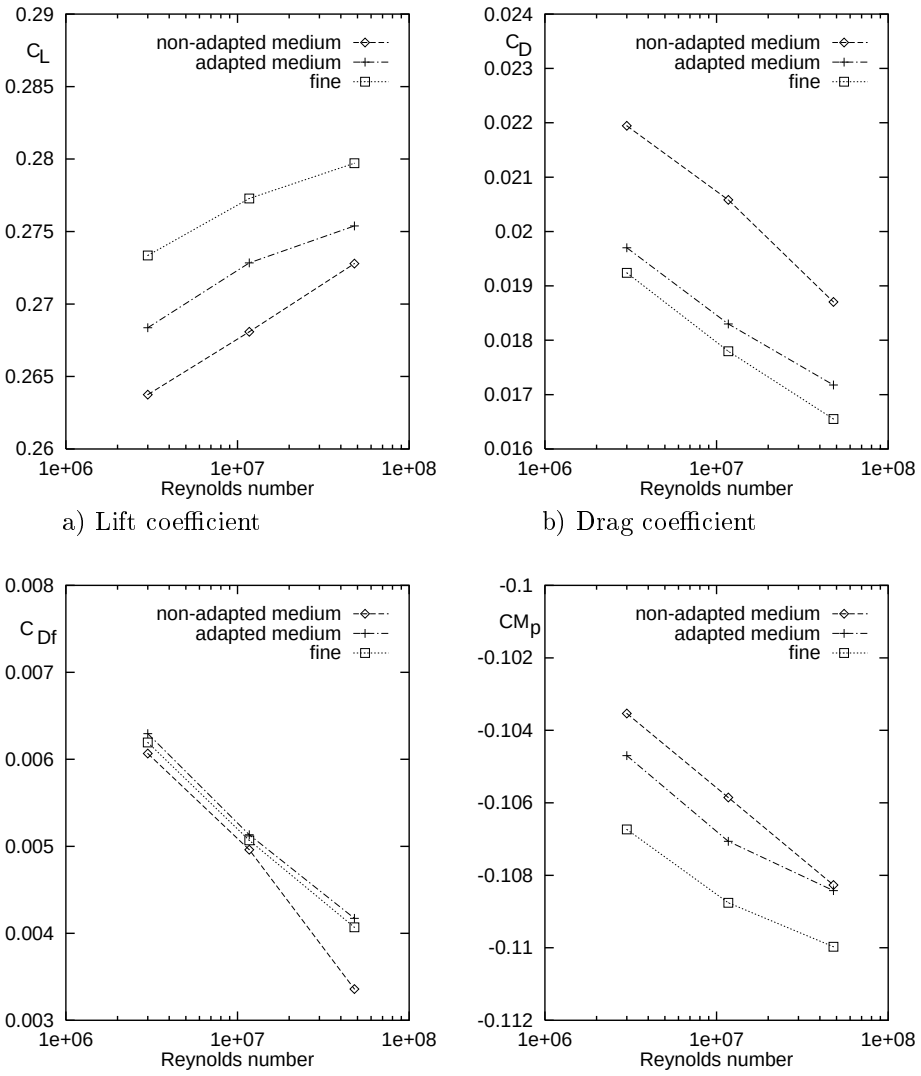

a) Lift coefficient

b) Drag coefficient

c) Friction drag coefficient

d) Pitch coefficient

Figure 6: Force coefficients as function of Reynolds number calculated on non-adapted and adapted medium grids, and calculated on fine grid.

References

[1] Löhner, R., *Mesh Adaptation in Fluid Mechanics*, Engineering Fracture Mechanics, **50**, No. 5/6, 819-847, 1995.

[2] Rubbert, P.E., *CFD and the changing world of airplane design*, ICAS Proceedings, 19th Congress of the International Council of the Aeronautical Sciences, September, 1994.

[3] Hagmeijer, R. , *Grid Adaption Based on Modified Anisotropic Diffusion Equations Formulated in the Parametric Domain*, Journal of Computational Physics, **115**, 169-183, 1994.

[4] Eiseman, P.R. , *Adaptive Grid Generation*, Computer Methods in Applied Mechanics and Engineering, **64** ,321-376, 1987

[5] Hagmeijer, R., *Anisotropic Grid Adaption Based on Diffusion Equations*, 4th International Conference on Numerical Grid Generation in Computational Fluid Dynamics and Related Fields, Swansea, UK 6-8th April 1994.

[6] Clement, Ph., Hagmeijer, R. and Sweers, G., *On the invertibility of Mappings arising in 2D Grid Generation Problems*, to appear in Numerische Mathematik.

[7] Barrett, Berry, Chan, Demmel, Donato, Dongarra, Eijkhout, Pozo, Romine, and van der Vorst, *Templates for the Solution of Linear Systems: Building Blocks for Iterative Methods* , SIAM Publications, 1993.

[8] Brandt, A., *Multi-Level adaptive Solutions to Boundary-Value Problems*, Math. Comp. **31** , 333-390, 1977.

[9] Schmitt, V. and Charpin, F., *Experimental Data Base for Computer Program Assessment* , AGARD-AR-138, 1979.

[10] Boerstoel, J.W., *ENFLOW a system of CFD codes for industrial CFD analysis of flows around aircraft including propulsion systems modelling* , NLR CR 93519 L, 1993

[11] Spekreijse, S.P., *Elliptic Grid Generation Based on Laplace Equations and Algebraic Transformations* , Journal of Computational Physics, **118**, 38-61, 1995.

[12] Kok, J.C., Amato, M., Bosse, S. and Kassies, A., *Numerical design of ENSOLV; a code for the numerical simulation of 3D flows using the thin-layer Navier-Stokes and Euler equations* , NLR CR 93152 L, 1993